International Journal of Non-Linear Mechanics 57 (2013) 168–175

Contents lists available at ScienceDirect

International Journal of Non-Linear Mechanics

journal homepage: www.elsevier.com/locate/nlm

Effect of variable permeability on the propagation of thin gravity currents in porous media

Valentina Ciriello [a,*], Vittorio Di Federico [a], Renata Archetti [a], Sandro Longo [b]

[a] Dipartimento di Ingegneria Civile, Chimica, Ambientale e dei Materiali (DICAM), Università di Bologna, Viale Risorgimento 2, 40136 Bologna, Italy
[b] Dipartimento di Ingegneria Civile, Ambiente Territorio e Architettura (DICATeA), Università di Parma, Italy

ARTICLE INFO

Article history:
Received 7 May 2013
Received in revised form
25 July 2013
Accepted 25 July 2013
Available online 2 August 2013

Keywords:
Porous
Gravity current
Similarity solution
Variable permeability

ABSTRACT

A new formulation is proposed to study the influence of deterministic heterogeneity on the propagation of thin two-dimensional gravity currents in a porous medium above a horizontal impervious boundary. Heterogeneity is conceptualized as a monotonic power-law variation of medium permeability transverse or parallel to the direction of propagation. Considering the injection of a constant or time-variable volume of fluid, the nonlinear differential problem admits a similarity solution which describes the shape and rate of propagation of the current. The bounds on parameters necessary to respect model assumptions are derived asymptotically and for finite time, to clarify the range of applicability of the proposed models. An application to the migration of a contaminant gravity current in the subsurface is then discussed, showing the impact of permeability variations on extension and shape of the intrusion.

1. Introduction

The understanding of gravity-driven flows in porous media is motivated by several environmental and geophysical applications, such as carbon dioxide sequestration, oil and gas reservoir exploitation, seawater intrusion, subsurface contamination and remediation of contaminated soils.

A variety of different models were proposed to conceptualize the configuration of possible natural settings of gravity driven flows in porous media [1]. Earlier works modeled plane or radial currents flowing in a homogeneous medium and driven by the free-surface gradient on a horizontal or inclined plane [2–4]. Later, additional details in the geometric description were provided by including the effect of impermeable confining boundaries [5], drainage by an underlying medium [6] or localized sink(s) (e.g. [7], and references therein), and varying topography [8]. Non-Newtonian power-law fluid rheology was also considered [9,10].

The subsurface environment exhibits spatial variation of the governing parameters on a multiplicity of scales; in turn, heterogeneity influences the propagation of gravity currents in several situations, such as long-term storage of carbon dioxide in geologic formations [11]. The ubiquitous presence of heterogeneity in natural media prompted the development of models of horizontal gravity currents considering deterministic variations of permeability and porosity in the vertical direction [2,12,13]; such trends may be positive or negative with distance from the surface, the latter being a more common case [14,15]. Likewise, permeability variations in the flow direction can affect the propagation behavior of gravity currents. Such horizontal spatial variations were considered in a number of groundwater problems, where a linear [16] or exponential [17] decrease in hydraulic conductivity with radial distance from a pumping well was conjectured to analyze steady-state tests. To describe the head response to fluid injection in a heterogeneous anticline reservoir, Yeh and Kuo [18] approximated the upper reservoir boundary with an abrupt change in thickness and hydraulic conductivity.

In this paper, we assess the influence of permeability varying transverse or parallel to the flow direction on the spreading of plane porous gravity currents driven by the instantaneous or maintained injection of a volume of fluid. Monotonic power-law variations with elevation or distance from the injection point provide a simplified description of heterogeneity. This formulation renders the problem amenable to a closed-form self-similar solution and generalizes results obtained for constant permeability by Huppert and Woods [2].

After formulating and solving the problem in dimensionless form for a vertical permeability variation, we discuss the limits placed on problem parameters by model assumptions (Section 2). A similar solution and analysis is presented in Section 3 for a horizontal permeability variation. An application involving the migration of a contaminant plume in a subsurface domain is included (Section 4), demonstrating the impact of permeability variations on the extension and shape of the intrusion. A set of conclusions (Section 5) closes the paper.

* Corresponding author. Tel.: +39 0512093753; fax: +39 0512093263.
E-mail addresses: valentina.ciriello3@unibo.it (V. Ciriello), sandro.longo@unipr.it (S. Longo).

0020-7462/$ - see front matter © 2013 Elsevier Ltd. All rights reserved.
http://dx.doi.org/10.1016/j.ijnonlinmec.2013.07.003

2. Vertical permeability variation

2.1. Theoretical developments

A gravity current of a fluid of density $\rho+\Delta\rho$ propagates under the action of gravity into a semi-infinite porous medium saturated with fluid of density ρ and confined by a lower horizontal impermeable boundary as depicted in Fig. 1. The volume (per unit width) of the intruding fluid increases with time as qt^{α}, q and α being both constant; $\alpha=0$ corresponds to the release of a constant volume, $\alpha=1$ to a constant flux. The permeability of the porous layer is assumed to vary vertically according to

$$k(z)=k_0(z/x^*)^{\omega-1}, \tag{1}$$

k_0 being the permeability at a reference length scale x^* and ω a numerical factor [19]; thus $\omega>1$ and $\omega<1$ represent respectively permeability increasing and decreasing with distance from the horizontal lower boundary; a porous medium with constant permeability k_0 corresponds to $\omega=1$, a case treated, among others, in Ref. [2]. We further set $\omega>\omega_1\equiv 0$, thus limiting the possible permeability rate of decrease with elevation.

The current height $h(x,t)$ describing the sharp interface between the intruding and ambient fluid varies with time t and distance x from the release point. In the following developments, we assume the typical current depth is much smaller than both its length and the depth of the reservoir h_0, thus allowing to neglect the motion of the ambient fluid and vertical velocities in the intruding fluid. With the further assumption that effects due to surface tension are negligible, the pressure distribution can then be taken to be hydrostatic.

Under these premises, Darcy's law yields in the horizontal direction $v(x,t)=-(k/\mu)\partial p/\partial x$, v being the Darcy velocity, p the pressure, μ the dynamic viscosity, and k the intrinsic permeability coefficient. The pressure within the incoming current is given by $p(x,z,t)=p_0+\Delta\rho g(h(x,t)-z)+\rho g(h_0-z)$, where $p_0=p(z=h_0)$ is a constant. Thus $\partial p/\partial x=\Delta\rho g(\partial h/\partial x)$ and coupling Darcy's law with (1) yields

$$v(x,z,t)=-(\Delta\rho g k_0/\mu)(z/x^*)^{\omega-1}\partial h/\partial x \tag{2}$$

For one dimensional transient flow, the local continuity condition takes the form [2]

$$\frac{\partial}{\partial x}\left(\int_0^h v\,dz\right)=-\phi\frac{\partial h}{\partial t}, \tag{3}$$

ϕ being the porosity. Substituting Eq. (2) into Eq. (3), the equation governing the evolution of the current height $h(x,t)$ is obtained as

$$\frac{1}{\omega}\frac{v^*}{(x^*)^{\omega-1}}\frac{\partial}{\partial x}\left[h^{\omega}\frac{\partial h}{\partial x}\right]=\frac{\partial h}{\partial t}, \tag{4}$$

where $v^*=\Delta\rho g k_0/\phi\mu$ is the characteristic velocity.

The boundary condition at the current front $x_N(t)$ and the global conservation of mass read respectively as

$$h(x_N(t),t)=0, \tag{5}$$

$$\phi\int_0^{x_N(t)}h(x,t)dx=qt^{\alpha}. \tag{6}$$

The previous equations can be rendered non-dimensional by setting, for $\alpha\neq 2$, $(x,x_N,z,t,h,v)=(x^*X,x^*X_N,x^*Z,t^*T,x^*H,v^*V)$, with capital letters representing the dimensionless variables and temporal, spatial and velocity scales given by $t^*=(q/(\phi v^{*2}))^{1/(2-\alpha)}$, $x^*=v^*t^*$, and v^* [10].

The non-dimensional versions of (4)–(6) then become

$$\frac{1}{\omega}\frac{\partial}{\partial X}\left[H^{\omega}\frac{\partial H}{\partial X}\right]=\frac{\partial H}{\partial T},\quad H(X_N(T),T)=0, \tag{7a, b}$$

$$\int_0^{X_N}H\,dX=T^{\alpha}. \tag{8}$$

Inspection of (7a,b) and (8) suggests the scalings $H^{\omega}\sim X^2/T$ and $HX\sim T^{\alpha}$; eliminating H yields the scale of the current length as $X\sim T^a$, while eliminating X gives $H\sim T^b$, with

$$a=\frac{\alpha\omega+1}{\omega+2},\quad b=\frac{2\alpha-1}{\omega+2} \tag{9a, b}$$

Guided by these scalings, a suitable similarity variable is defined as (the prefactor ω^c is inserted to render subsequent expressions simpler)

$$\eta=\omega^c X/T^a,\quad c=\frac{1}{\omega+2} \tag{10a, b}$$

and a similarity solution is sought in the form $H(X,T)=\omega^c T^b f(\eta)$, where the constant $\eta_N(\alpha,\omega)$ denotes the value of η at the current front. Rescaling η as $\zeta=\eta/\eta_N$ and $f(\eta)$ as $f(\eta)=\eta_N^d\Psi(\zeta)$, where

$$d=2/\omega, \tag{11}$$

the similarity solution of Eqs. (7a,b) and (8) is of the form

$$H(X,T)=\omega^c\eta_N^d T^b\Psi(\zeta). \tag{12}$$

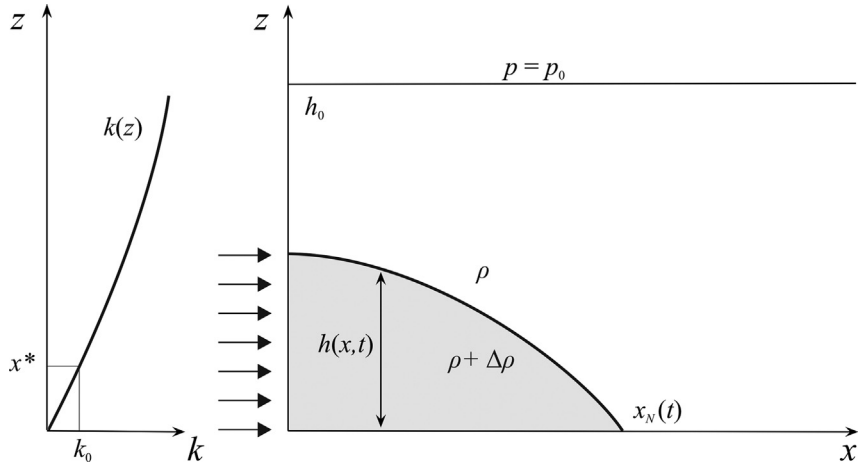

Fig. 1. Flow domain.

Substituting these expressions in governing dimensionless equations yields the following expressions:

$$\frac{d}{d\zeta}\left[\Psi^{\omega}\frac{d\Psi}{d\zeta}\right]+a\zeta\frac{d\Psi}{d\zeta}-b\Psi=0,\quad \Psi(1)=0, \tag{13a, b}$$

$$\eta_N=\left(\int_0^1\Psi(\zeta)d\zeta\right)^{-\omega/(\omega+2)}. \tag{14}$$

Solution of (13a,b) yields the shape function $\Psi(\zeta)$, while (14) provides the prefactor $\eta_N(\alpha,\omega)$. Once $\Psi(\zeta)$ and η_N are determined, the length of the gravity current and the velocity field are given by

$$X_N(T)=\frac{\eta_N}{\omega^c}T^a, \tag{15}$$

$$V(Z,T,\zeta)=-\phi\omega^{2c}\eta_N^{(2-\omega)/\omega}Z^{\omega-1}T^{[\alpha(2-\omega)-2]/(\omega+2)}\frac{d\Psi}{d\zeta}. \tag{16}$$

For $\omega=1$, governing equations and results reduce to their simpler counterparts derived in dimensional form by Huppert and Woods [2] for horizontal flow in a homogeneous medium; numerical factors defined earlier reduce to $a=(\alpha+1)/3$, $b=(2\alpha-1)/3$, $c=1/3$, $d=2$.

For $\alpha=0$ the solution of (13a,b) and (14) can be obtained analytically as

$$\Psi(\zeta)=\left[\frac{\omega}{2(\omega+2)}(1-\zeta^2)\right]^{1/\omega}, \tag{17}$$

$$\eta_N=\left[\frac{2(\omega+2)}{\omega}\right]^{1/(\omega+2)}\left[\frac{(\omega+2)\Gamma\left(\frac{\omega+2}{2\omega}\right)}{\sqrt{\pi}\quad\Gamma\left(\frac{1}{\omega}\right)}\right]^{\omega/(\omega+2)}. \tag{18}$$

For the constant permeability case $\omega=1$, Eqs. (17) and (18) reduce to $\Psi(\zeta)=(1-\zeta^2)/6$ and $\eta_N=(9)^{1/3}$ as first derived by Pattle [20].

The behavior of the solution to Eq. (13a,b) near the current front $\zeta\approx1$ is given by the expressions (see Appendix for a detailed derivation)

$$\frac{d\Psi}{d\zeta}(\zeta\approx1)=-\frac{1}{\omega}\left(\frac{\alpha\omega^2+\omega}{\omega+2}\right)^{1/\omega}(1-\zeta)^{1/\omega-1}, \tag{19}$$

$$\Psi(\zeta\approx1)=\left(\frac{\alpha\omega^2+\omega}{\omega+2}\right)^{1/\omega}(1-\zeta)^{1/\omega}. \tag{20}$$

Shape factors $\Psi(\zeta)$ resulting from numerical integration of Eq. (13a) with boundary conditions (13b) and (19) with Wolfram Mathematica® 7 are depicted in Fig. 2a,b respectively for $\alpha=0$ and 1 and different values of ω. For $\alpha=0$, numerical results reproduce the analytical solution (17).

It is seen that the shape factor decidedly increases as ω increases from values below to values above unity, implying a positive rather than negative trend of the permeability with elevation. For a given permeability variation with elevation (fixed ω), the shape factor increases with α, i.e. the fluid volume released into the domain; this is so also for values of $\alpha>1$ (not shown).

In Fig. 2c a graph of η_N, evaluated via Eq. (14), is depicted as a function of α for different values of ω. This pre-multiplicative factor is seen to decrease as α and ω increase; the dependence of η_N on the value of ω is more marked for $\omega<1$.

For $\alpha=2$, the dimensionless formulation adopted breaks down for lack of the time scale t^*, while a second velocity scale $(q/\phi)^{1/2}$ arises. This case can be treated introducing new hatted dimensionless variables [10] as $(x,x_N,z,t,h,v)=(\hat{x}^*\hat{X},\hat{x}^*\hat{X}_N,\hat{x}^*\hat{Z},\hat{t}^*\hat{T},\hat{x}^*\hat{H},V^*\hat{V})$, where an arbitrary time scale $\hat{t}^*$ is adopted, and the new spatial scale is $\hat{x}^*=(q/\phi)^{1/2}\hat{t}^*$. This leads to Eqs. (7a,b) and (8) being replaced by

$$\frac{\delta}{\omega}\frac{\partial}{\partial\hat{X}}\left[\hat{H}^{\omega}\frac{\partial\hat{H}}{\partial\hat{X}}\right]=\frac{\partial\hat{H}}{\partial\hat{T}},\quad \int_0^{\hat{X}_N}\hat{H}\,d\hat{X}=\hat{T}^2,\quad \hat{H}(\hat{X}_N(\hat{T}),\hat{T})=0, \tag{21a, b, c}$$

where $\delta=v^*/(q/\phi)^{1/2}$ is the ratio between the two velocity scales in the problem.

The self-similar variable is defined as $\eta=\beta^c\hat{X}/\hat{T}^a$, with $a=(2\omega+1)/(\omega+2)$, $c=1/(\omega+2)$. Performing the same mathematical manipulations as in the general case, the current height becomes $\hat{H}(\hat{X},\hat{T})=\omega^c\eta_N^d\hat{T}^b\Psi(\zeta)$, where $\zeta=\eta/\eta_N$, $b=3/(\omega+2)$, $d=2/\omega$, and the shape factor Ψ is obtained solving

$$\delta\frac{d}{d\zeta}\left[\Psi^{\omega}\frac{d\Psi}{d\zeta}\right]+a\zeta\frac{d\Psi}{d\zeta}-b\Psi=0, \tag{22}$$

with boundary condition (21c), while (14) remains unchanged.

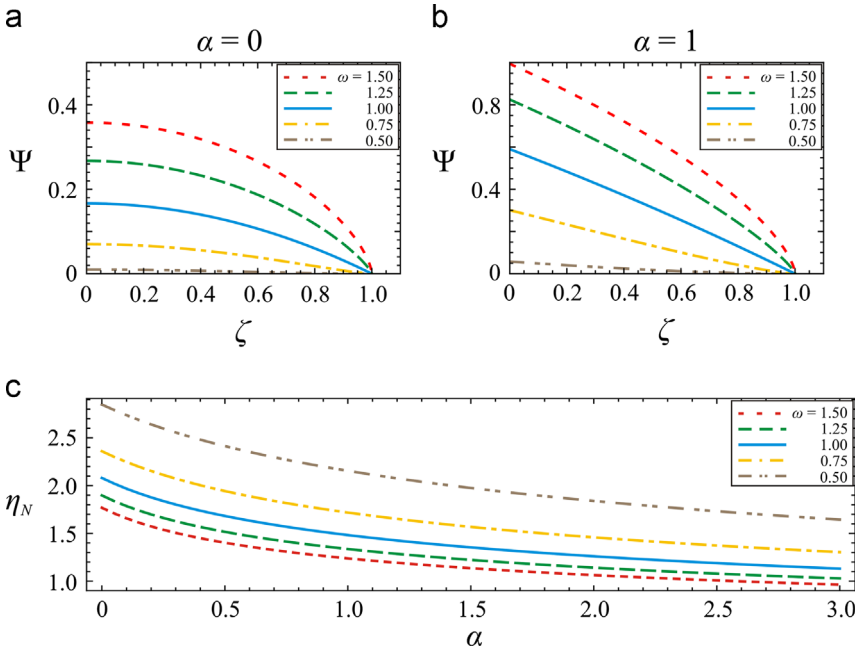

Fig. 2. Solution of (13a,b) and (14) for different values of ω: (a) shape factor for instantaneous injection ($\alpha=0$); (b) shape factor for constant injection ($\alpha=1$); (c) prefactor $\eta_N(\alpha,\omega)$.

2.2. Discussion and limits of validity

In this sub-section we analyze the physical limits of validity of the solutions previously derived for vertically varying permeability. We first note that given the initial limit imposed on the permeability variation $\omega > \omega_1 \equiv 0$, it follows that $a > 0$, i.e. the expression (15) of the distance of propagation $X_N(T)$ retains its physical meaning. Hence the front velocity is proportional to $T^{a-1} = T^{[\omega(\alpha-1)-1]/(\omega+2)}$, i.e. the current decelerates or accelerates depending whether $0 < \alpha < \alpha_c$ or $\alpha > \alpha_c$, with $\alpha_c = (\omega+1)/\omega$. For homogeneous media ($\omega = 1$), the value $\alpha_c = 2$ is recovered; for a very rapid permeability increase ($\omega \to \infty$), α_c tends to unity. Conversely, for given $\alpha > 1$, the current can be accelerated only for $\omega > \omega_c = 1/(\alpha-1)$.

Upon examining Eq. (12), it is seen that the current height increases or decreases with respect to time depending on whether $b > 0$ or $b < 0$; in the former case, the assumption of a thin current with respect to the ambient porous medium ($h \ll h_0$) is eventually violated, and flow of the ambient fluid must be taken into account. Hence $0 < \alpha < \alpha_1 \equiv 1/2$ is required for the solution to be asymptotically valid [5].

Furthermore, as the free-surface gradient is given by

$$\partial h/\partial x = \partial H/\partial X = \omega^{2c} \eta_N^{d-1} T^{b-a} d\Psi(\zeta)/d\zeta, \tag{23}$$

the condition $b-a = [(2-\omega)\alpha - 2]/(\omega+2) < 0$ must be satisfied for the requirement of modest surface curvature $\partial h/\partial x \ll 1$ to hold asymptotically, with the further assumption that the gradient of the shape function is limited. In turn, given that $\omega > \omega_1 \equiv 0$, this condition implies $\alpha < \alpha_2 \equiv 2/(2-\omega)$, but this constraint is less stringent than $\alpha < \alpha_1 \equiv 1/2$. It is noted that the physical limitation $\alpha > 0$ is satisfied for $\omega < \omega_2 \equiv 2$, i.e., for permeability decreasing ($\omega < 1$), or increasing less than linearly ($\omega < 2$), along the vertical; this constitutes an upper bound ω_2 to the value of ω.

Finally, the ratio between current height and overall length yields $h(x,t)/x_N(t) = H(X,T)/X_N(T) = \omega^{2c} \eta_N^{d-1} T^{b-a} \Psi(\zeta)$, hence the thin current approximation $h/x_N \ll 1$ requires asymptotically the same bounds derived earlier from Eq. (23), with the further assumption that the shape function is limited. The previous limits on parameters are summarized in Fig. 3; it is seen that only decelerated currents with $\alpha < 1/2$ in porous media with $0 < \omega < 2$ satisfy all model assumptions.

A more realistic analysis requires the evaluation of the limits at finite times. We exemplify our approach by requiring that $\partial h/\partial x = \varepsilon \ll 1$ at time T. The necessary conditions can be reformulated introducing in Eq. (23) the average gradient of the shape function at a given time, equal to $(d\Psi/d\zeta)_{avg} = 2T^{\alpha}/X_N^2 \equiv 2\omega^{2/(\omega+2)} T^{\alpha-2a}/\eta_N^2$; hence

$$\partial h/\partial x = \partial H/\partial X = 2\omega^{4/(\omega+2)} \eta_N^{(2-3\omega)/\omega} T^{[\alpha(4-2\omega)-4]/(\omega+2)}, \tag{24}$$

and

$$\alpha < \alpha_2 + \frac{\omega+2}{4-2\omega} \ln\left(\frac{\varepsilon \eta_N^{(3\omega-2)/\omega}}{2\omega^{4/(\omega+2)}}\right) / \ln T. \tag{25}$$

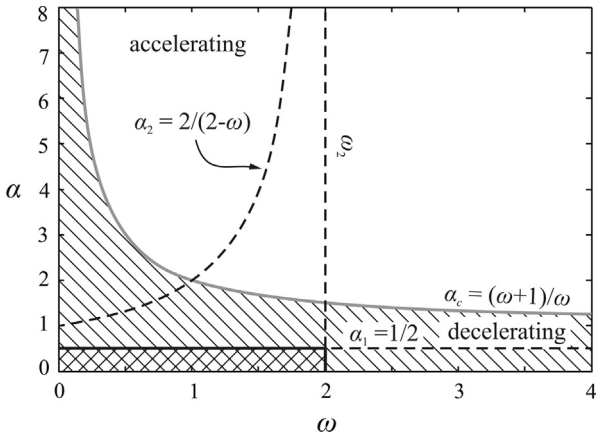

Fig. 3. Asymptotic limits of validity of the analysis for a vertical variation of permeability. The cross-hatched area represents the domain of variability of parameters satisfying all model assumptions.

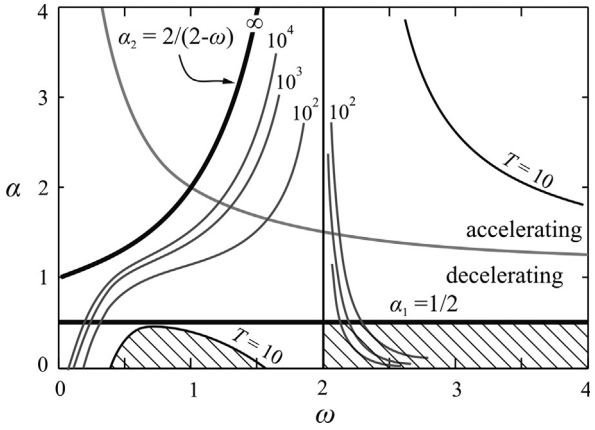

Fig. 4. Time dependent limits of validity of the analysis for a vertical variation of permeability to satisfy $\partial h/\partial x = \varepsilon \ll 1$, $\varepsilon = 0.1$. The hatched area represents the domain of variability of parameters satisfying all model assumptions at $T = 10$.

Fig. 4 shows the limit curves given by Eq. (25), computed numerically for $T = 10$, 100, 1000, 10,000 and $\varepsilon = 0.1$.

The bounds for finite times allow both accelerated and decelerated currents satisfying the condition on the gradient. For $\omega < 2$, larger values of α are allowed as time T increases, with the upper limit value α_2 asymptotically reached for $T \to \infty$, even though the limit α_1 becomes soon dominant. The reverse is true for $\omega > 2$; asymptotically, the latter case does not satisfy the condition on the gradient. Note that different curves could be obtained assuming a different criterion to evaluate the gradient of the shape function (e.g. a threshold value valid for at least 80% of the current length could be chosen instead of the average gradient herein adopted) and/or a different value of ε, but the scenario is qualitatively similar.

The limits to be imposed on parameters/time to satisfy the requirement $h \ll h_0$ are best considered for a given value of h_0 in a specific application (see Section 4); if the ambient fluid is air, h_0 is virtually infinite.

3. Horizontal permeability variation

3.1. Theoretical developments

In the following a horizontal (e.g. in the direction of propagation) permeability variation is assumed to occur according to

$$k(x) = k_0 (x/x^*)^{\beta}, \tag{26}$$

k_0 again being the permeability at a reference length scale x^* and β a numerical factor; thus $\beta > 0$ and $\beta < 0$ represent respectively permeability increasing and decreasing with horizontal distance from the source, the latter being a more common case [16,17]; the case $\beta = 0$ represents a homogeneous medium. A similar approach was adopted in Ref. [21] for the analysis of viscous gravity currents in channels of given shape, allowing the parameter associated with the channel width to vary with a power-law dependence on distance from the source.

Under the same assumptions of the vertical variability case, the equation governing the evolution of the current height, taking

Darcy's law into account, is

$$v^* \frac{\partial}{\partial x}\left[\left(\frac{x}{x^*}\right)^{\beta} h \frac{\partial h}{\partial x}\right] = \frac{\partial h}{\partial t}, \tag{27}$$

with boundary condition (5), together with the global continuity Eq. (6). Switching to the dimensionless variables defined earlier yields, for $\alpha \neq 2$,

$$\frac{\partial}{\partial X}\left[X^{\beta} H \frac{\partial H}{\partial X}\right] = \frac{\partial H}{\partial T} \tag{28}$$

and two equations identical to Eqs. (7a,b) and (8). In this case the appropriate scalings for the current length and height are $X \sim T^a$ and $H \sim T^b$, with

$$a = \frac{\alpha+1}{3-\beta}, \quad b = \frac{\alpha(2-\beta)-1}{3-\beta} \tag{29a, b}$$

The similarity variable is defined as $\eta = X/T^a$, and a similarity solution is sought in the form $X_N(T) = \eta_N T^a$, $H(X,T) = T^b f(\eta)$, where $\eta_N(\alpha,\beta)$ is the value of η at the current front. Rescaling of η as $\zeta = \eta/\eta_N$ and of $f(\eta)$ as $f(\eta) = \eta_N^d \Psi(\zeta)$, where $d = 2-\beta$, gives the similarity solution in terms of current height as

$$H(X,T) = \eta_N^d T^b \Psi(\zeta). \tag{30}$$

Thus the differential problem transforms into

$$\frac{d}{d\zeta}\left[\zeta^{\beta}\Psi\frac{d\Psi}{d\zeta}\right] + a\zeta\frac{d\Psi}{d\zeta} - b\Psi = 0, \quad \Psi(1) = 0, \tag{31a, b}$$

$$\eta_N = \left(\int_0^1 \Psi(\zeta) d\zeta\right)^{-1/(3-\beta)}. \tag{32}$$

Once $\Psi(\zeta)$ and η_N are determined, dimensionless velocity is given by $V(X,T,\zeta) = -\phi\eta_N^{1-\beta} X^{\beta} T^{[\alpha(1-\beta)-2]/(3-\beta)} (d\Psi/d\zeta)$.

For $\beta = 0$, earlier results for a homogeneous medium are recovered. A closed-form solution to Eq. (31a,b) and (32) is readily available for $\alpha = 0$ as

$$\Psi(\zeta) = \frac{1}{(3-\beta)(2-\beta)}(1-\zeta^{2-\beta}), \tag{33}$$

$$\eta_N = (3-\beta)^{2/(3-\beta)} \tag{34}$$

which holds for $\beta < 2$. For a homogeneous medium ($\beta = 0$), Eqs. (33) and (34) again reduce to $\Psi(\zeta) = (1-\zeta^2)/6$ and $\eta_N = (9)^{1/3}$.

Near $\zeta = 1$ the following approximate expressions can be derived

$$\frac{d\Psi}{d\zeta}(\zeta \approx 1) = -\frac{\alpha+1}{3-\beta}\zeta^{1-\beta}, \tag{35}$$

$$\Psi(\zeta \approx 1) = \frac{\alpha+1}{(2-\beta)(3-\beta)}(1-\zeta^{2-\beta}). \tag{36}$$

Shape factors $\Psi(\zeta)$ resulting from numerical integration of Eq. (31a) with boundary conditions (31b) and (35) are depicted in Fig. 5a and b respectively for $\alpha = 0$ and 1 and different values of β. For $\alpha = 0$, numerical results reproduce the analytical solution (33) and (34). Shape factors increase as β increases, doing so more rapidly near the injection point for $\beta > 0$; for a constant injection rate ($\alpha = 1$) and permeability increasing in space, the profiles are concave rather than convex. For a given permeability variation, the shape factor increases with α, i.e. the fluid volume released into the domain. The prefactor η_N, calculated via Eq. (32), is depicted in Fig. 5c as a function of α for different values of β. This pre-multiplicative factor is seen to decrease as α increases, more so for $\beta > 0$ than for $\beta < 0$; the dependence of η_N on the value of β is more marked for permeability increasing than decreasing with distance.

For $\alpha = 2$, a different dimensionless formulation is needed, identical to that described earlier for a vertical permeability variation. The corresponding governing equations are

$$\delta\frac{\partial}{\partial \hat{X}}\left[\hat{X}^{\beta}\hat{H}\frac{\partial H}{\partial \hat{X}}\right] = \frac{\partial \hat{H}}{\partial \hat{T}}, \tag{37}$$

and (21b,c). The self-similar variable and current height are given by $\eta = \hat{X}/\hat{T}^a$, $\hat{H}(\hat{X},\hat{T}) = \eta_N^d \hat{T}^b \Psi(\zeta)$, with $a = 3/(3-\beta)$, $b = (3-2\beta)/(3-\beta)$, $d = 2-\beta$, while the shape factor Ψ is derived solving

$$\delta\frac{d}{d\zeta}\left[\zeta^{\beta}\Psi\frac{d\Psi}{d\zeta}\right] + a\zeta\frac{d\Psi}{d\zeta} - b\Psi = 0. \tag{38}$$

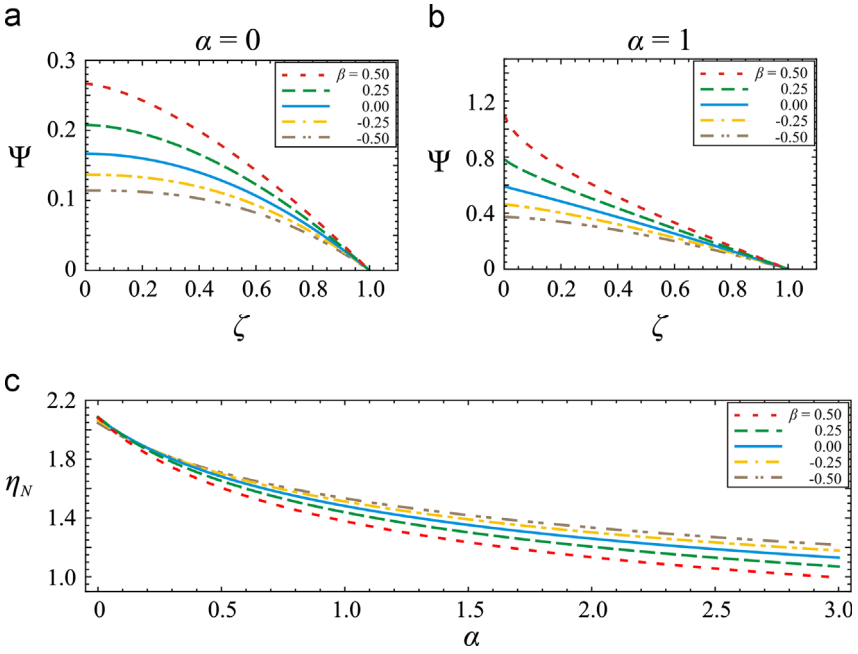

Fig. 5. Solution of (31a,b) and (32) for different values of β: (a) shape factor for instantaneous injection ($\alpha = 0$); (b) shape factor for constant injection ($\alpha = 1$); (c) prefactor $\eta_N(\alpha,\beta)$.

3.2. Discussion and limits of validity

Following our earlier analysis for currents in media with vertically varying permeability, we observe that for the expression of the distance of propagation $X_N(T)$ to retain its physical meaning, it must be $a>0$, whence it follows that $\beta<\beta_1\equiv 3$, i.e. there is an upper limit to the increase of the permeability in the horizontal direction. If this condition is respected, the velocity of the front is proportional to $t^{a-1}=t^{(\alpha+\beta-2)/(3-\beta)}$, i.e. the current decelerates or accelerates depending whether $0<\alpha<\alpha_c$ or $\alpha>\alpha_c$, with $\alpha_c=2-\beta$. Conversely, for given α, the current accelerates or decelerates for $\beta<\beta_c$ or $\beta_c<\beta<\beta_1$, with $\beta_c=2-\alpha$.

As earlier noted, asymptotic validity of the thin current assumption requires $b<0$, implying the condition $0<\alpha<\alpha_1\equiv 1/(2-\beta)$, or, conversely, $2-1/\alpha<\beta<\beta_1$; for $\beta=0$, this reduces to $\alpha<1/2$. The physical constraint $\alpha>0$ is satisfied for $\beta<\beta_2\equiv 2$.

Moreover, limitations on the gradient $\partial h/\partial x=\partial H/\partial X=\eta_N^{d-1}T^{b-a}\,d\Psi(\zeta)/d\zeta$ require $b-a=[(1-\beta)\alpha-2]/(3-\beta)<0$. In turn, given the previous limit $\beta<\beta_1\equiv 3$, this is equivalent to $\alpha<\alpha_2\equiv 2/(1-\beta)$; this constraint is less stringent than $\alpha<\alpha_1\equiv 1/(2-\beta)$. It is noted that the physical limitation $\alpha>0$ is satisfied for $\beta<\beta_3\equiv 1$, i.e., for permeability decreasing ($\beta<0$), or increasing less than linearly, along the x axis; this third upper bound β_3 to the value of β is more stringent than β_1 and β_2. The greater the value of β below β_3, the larger the value of α_1; when the permeability increases moderately ($0<\beta<\beta_3\equiv 1$) α_1 can reach the maximum value 1. For spatially decreasing permeability ($\beta<0$), the fluid is progressively slowed, and the current can remain thin only when $\alpha<\alpha_1<1/2$; e.g. $\alpha_1=1/3$ for $\beta=-1$. Conversely, for a given rate α of increase of fluid volume with time, it must be $(2\alpha-1)/\alpha<\beta<\beta_3$. For an instantaneous injection ($\alpha=0$), β has no lower bound (however there is an upper one $\beta<\beta_3\equiv 1$), while for an injection with a constant flow rate ($\alpha=1$) only the single value $\beta=\beta_3\equiv 1$ is allowed to satisfy the multiple constraints.

These asymptotic limits are summarized in Fig. 6; only decelerated currents in media with $\beta<1$ and release rate $\alpha<1/(2-\beta)$ satisfy all model assumptions.

Conducting the analysis at a finite time T along the previous lines yields for the condition on the free surface curvature

$$\partial h/\partial x=\partial H/\partial X=2\eta_N^{-1-\beta}T^{[2\alpha(1-\beta)-4]/(3-\beta)}<\varepsilon, \tag{39}$$

giving in turn the bound

$$\alpha<\alpha_2+\frac{3-\beta}{2-2\beta}\ln\left(\frac{\varepsilon\eta_N^{1+\beta}}{2}\right)/\ln T. \tag{40}$$

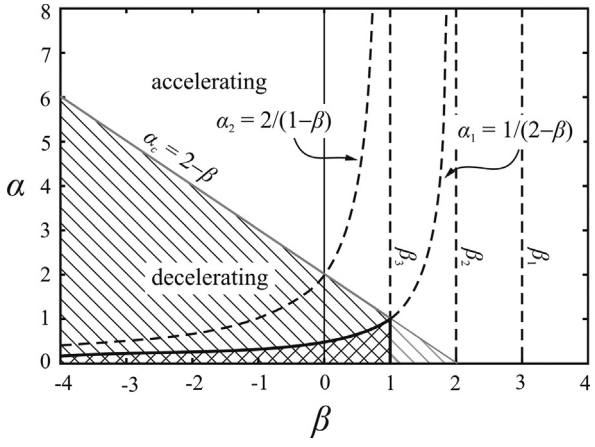

Fig. 6. Asymptotic limits of validity of the analysis for an horizontal variation of permeability. The cross-hatched area represents the domain of variability of parameters satisfying all model assumptions.

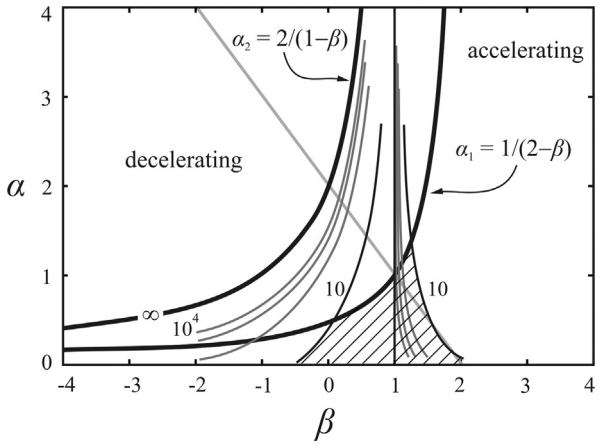

Fig. 7. Time dependent limits of validity of the analysis for an horizontal variation of permeability to satisfy $\partial h/\partial x=\varepsilon\ll 1$, $\varepsilon=0.1$. The hatched area represents the domain of variability of parameters satisfying all model assumptions at $T=10$.

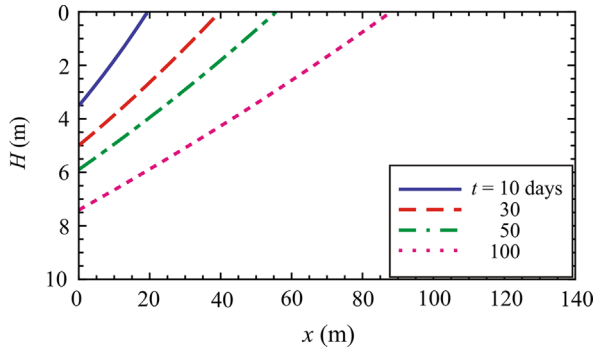

Fig. 8. Current profiles at $t=10$, 30, 50 and 100 days for problem parameters as in Section 4, constant permeability.

Fig. 7 shows the limit curves given by (40), computed numerically for $T=10$, 100, 1000, 10,000 and $\varepsilon=0.1$.

The bounds for finite times indicate that a limit more stringent than the asymptotic one can arise with respect to α_1 and α_2. For $\beta<1$, larger values of α are allowed as time T increases, with the upper limit value α_2 asymptotically reached for $T\to\infty$. For $\beta>1$ lower values of α and β are allowed as time T increases, with the limit $\beta=1$ reached asymptotically. Hence accelerated currents with a permeability increasing horizontally more than linearly are admitted at short times.

4. An example application

In the following the derived models are applied to illustrate the impact of vertical or horizontal permeability variations in a hypothetical application involving contaminant spreading in a subsurface environment. Assume that at $t=0$ a spill of gasoline initiates with constant flow rate from a large tank near the upper portion of a confined sandy aquifer $h_0=20$ m thick and saturated with water. Thus the situation represented in Fig. 1 is reversed (see Figs. 8–10) and the buoyant gasoline plume propagates on top of the water, flowing below the impermeable aquifer roof; $\omega<1$ and $\omega>1$ here imply respectively permeability decreasing and increasing with depth. We assume as problem parameters a gasoline density $\rho=870$ kg/m^3 [22], and viscosity $\mu=6\times 10^{-4}$ Pa s; a water density $\rho+\Delta\rho=1000$ kg/m^3; an aquifer porosity $\phi=0.3$; a characteristic permeability $k_0=10^{-11}$ m^2; a constant rate of injection ($\alpha=1$) under an impervious layer; a release rate $q=1$ m^3/m/day $\cong 1.16\times 10^{-5}$ m^2/s. The propagation of the gasoline plume in a subsurface setting having

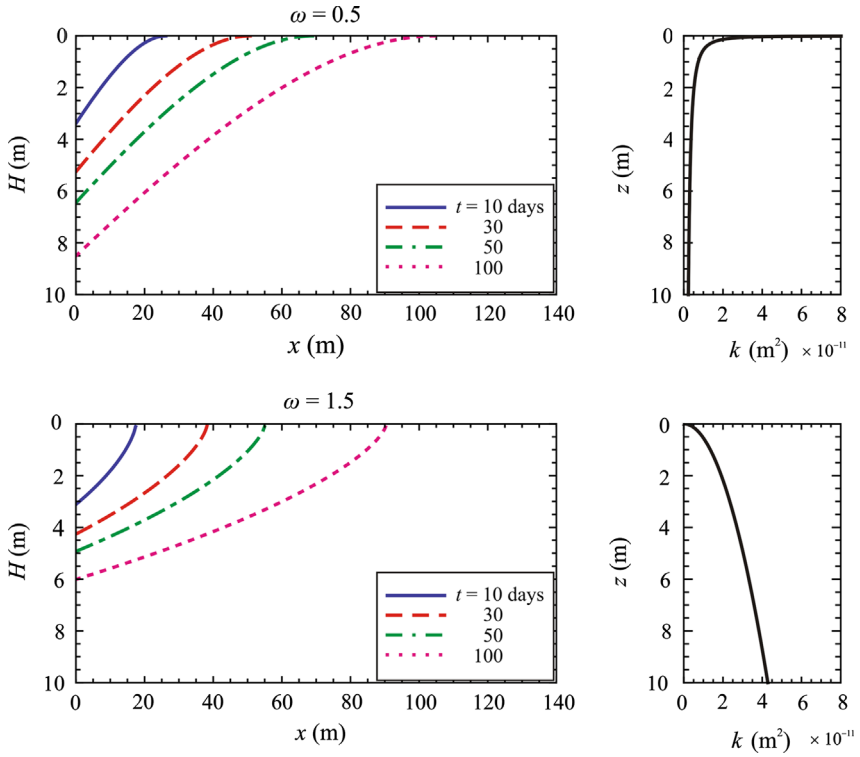

Fig. 9. Current profiles as in Fig. 8 but with vertical permeability variation: (a) $\omega = 0.50$; (b) $\omega = 1.50$.

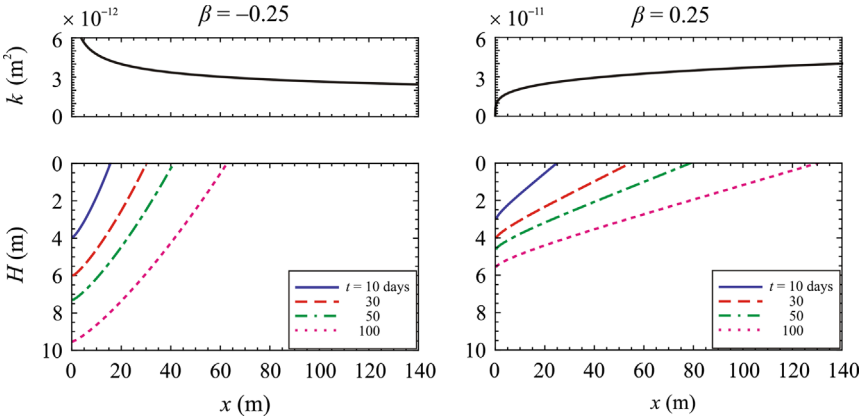

Fig. 10. Current profiles as in Fig. 8 but with horizontal permeability variation: (a) $\beta = -0.25$; (b) $\beta = 0.25$.

constant permeability k_0 (reference case 0) is then compared with that resulting from a permeability variation described by (1), with ω taken to be either 0.50 (case a) or 1.50 (case b), to represent a decrease or increase of permeability with depth. For the parameters listed above, the velocity, length and time scales are respectively equal to $v^* = 7.26 \times 10^{-5}$ m/s, $x^* = 0.54$ m, $t^* = 0.09$ days, implying, according to Eq. (1), permeability variations over the aquifer thickness within one order of magnitude from k_0.

Figs. 8 and 9a–b depict the height profiles as a function of time respectively for the reference case (0) and cases (a)–(b), for times $t_1 = 10$ days, $t_2 = 30$ days, $t_3 = 50$ days, $t_4 = 100$ days. It is noted that for short times the current advances farthest for $\omega < 1$ and slowest for $\omega > 1$: after 10 days $x_{Na}(t_1) = 26.3$ m, $x_{N0}(t_1) = 18.8$ m, $x_{Nb}(t_1) = 17.5$ m, with a relative difference of $\approx +40\%$ and $\approx -7\%$ for cases (a) and (b) with respect to case (0). This difference is due to the different values of permeability encountered by the current front in the top portion of the aquifer, which are respectively larger and smaller than the reference permeability. However as the intruding current grows in size, it reaches lower portions of the aquifer having permeability values smaller than k_0 for $\omega < 1$ and higher for $\omega > 1$. This brings about an increase in the current velocity for $\omega > 1$, and a decrease for $\omega < 1$: after 100 days $x_{Na}(t_4) = 104.8$ m, $x_{N0}(t_4) = 87.3$ m, $x_{Nc}(t_1) = 90.7$ m, i.e. the current within the homogeneous aquifer is the slowest. For much larger values of time, the situation is reversed, and currents propagating in media with permeability increasing with depth (case b) become faster than for cases (0) and (a).

Correspondingly, heterogeneity significantly modifies the shape of the intruding current. Profiles for case (a) have a moderately larger depth in the origin than those for cases (0) and (b), but affect a smaller portion of the domain near the front due to their shape. It is noted that around $t_4 = 100$ days, the average current depth reaches values comparable in magnitude with the aquifer's, requiring consideration of motion in the ambient fluid.

Fig. 10a, b illustrates the propagation of a gravity current under the same assumptions of the previous example, except that a horizontal permeability trend is considered according to (26), with β taken to be either -0.25 (case a) or 0.25 (case b), to represent

decreasing or increasing permeability along the direction of propagation. Currents in media with decreasing or increasing permeability are respectively slower and faster than in the homogeneous case; the positions reached by the front at 100 days are $x_{Na}(t_4)=62.1$ m and $x_{Nb}(t_4)=129.4$ m, with a relative difference of $\approx -29\%$ and $\approx 49\%$ for cases (a) and (b) with respect to case (0). At these distances from the injection point, the permeability in cases (a) and (b) is $k(x_{Na})=3.03\times10^{-12}$ m^2, $k(x_{Nb})=3.93\times10^{-11}$ m^2, with a relative variation of $\approx -69\%$ and $\approx 292\%$ with respect to k_0. These variations are still realistic; for larger scales, the positive trend in permeability is not physically plausible.

The shape of intruding currents is significantly affected also for horizontally varying permeability. Profiles are steeper and with a larger average depth for permeability decreasing with distance from the injection point than for constant or increasing permeability; correspondingly, their average depth reaches sooner values comparable in magnitude with the aquifer thickness.

5. Conclusions

A general analytical formulation to describe the spreading of plane viscous gravity currents in porous media is derived under conditions of permeability varying transverse or parallel to the direction of propagation. The description of heterogeneity via a monotonic power-law variation may represent a suitable idealization of real situations, and allows derivation of the rate of spreading and the current profile in self-similar form, generalizing results valid for constant permeability. Limitations on parameters necessary to respect rigorously model assumptions are included to complete the formulation and clarify its range of practical applicability. Results are firstly discussed in a general dimensionless framework and then analyzed in dimensional form to assess model applicability to groundwater contamination by an intruding plume. In this way we verify how heterogeneity can decidedly alter the rate of spreading of horizontal gravity currents, as demonstrated by Silin et al. [23] for vertical CO_2 migration. Spatial variations in permeability influence also the current profile, steepness and average height. Their assessment is relevant when the overall extent and shape of the domain affected by the advancing current needs to be determined, e.g. for CO_2 or contaminant spreading, in-situ soil remediation, saltwater intrusion.

Appendix

The aim of this Appendix is to derive an asymptotic solution to (13a,b) near the current tip ($\zeta=1$) in the form of a series expansion of the shape factor, to be used as a second boundary condition in its numerical integration. Upon introducing the variable $\chi=1-\zeta$, Eq. (13a,b) transforms into

$$\frac{d}{d\chi}\left[\Psi^{\omega}\frac{d\Psi}{d\chi}\right]-a(1-\chi)\frac{d\Psi}{d\chi}-b\Psi=0,\quad \Psi(\chi\to0)=0. \tag{A.1a, b}$$

An approximate solution to (A.1a) satisfying (A.1b) is sought in the form of a Frobenius series with indicial exponent r

$$\Psi(\chi)=\sum_{k=0}^{\infty}a_k\chi^{k+r}. \tag{A.2}$$

The derivative and the ωth power of (A.2) are respectively equal to

$$\frac{d\Psi}{d\chi}=\sum_{k=0}^{\infty}a_k(k+r)\chi^{k+r-1} \tag{A.3}$$

$$\Psi^{\omega}=\sum_{m_0,m_1,\ldots m_k}\binom{\omega}{m_0,m_1,\ldots,m_k}(a_0\chi^r)^{m_0}\cdot[a_1\chi^{r+1}]^{m_1}\cdot\cdots\cdot[a_k\chi^{k+r}]^{m_k}$$
$$=a_0^{\omega}\chi^{r\omega}+\ldots \tag{A.4}$$

where the summation is taken over all sequences of indices m_0 through m_k, such that the sum of all m_k is equal to ω. The multinomial coefficients can be computed as

$$\binom{\omega}{m_0,m_1,\ldots,m_k}=\frac{\omega!}{m_0!m_1!\cdot\cdots\cdot m_k!} \tag{A.5}$$

Substituting (A.3)–(A.4) in Eq. (A.1a) the following expression is obtained:

$$a_0^{\omega+1}r[r(\omega+1)-1]\chi^{r(\omega+1)-2}+\ldots-a\sum_{k=0}^{\infty}a_k(r+k)\chi^{r+k-1}$$
$$+a\sum_{k=0}^{\infty}a_k(r+k)\chi^{r+k}-b\sum_{k=0}^{\infty}a_k\chi^{(r+k)}=0, \tag{A.6}$$

writing in explicit form only the first term in the expansion of Ψ^{ω}. Equating the lowest powers of χ (for $k=0$) we find the indicial exponent to be $r=1/\omega$; equating the coefficients of the different powers of χ to zero, all the coefficients a_k are derived. In particular, the first coefficient is

$$a_0=(a\omega)^{1/\omega}. \tag{A.7}$$

Eqs. (19) and (20) are easily derived from (A.7).

References

[1] H.E. Huppert, Gravity currents: a personal perspective, Journal of Fluid Mechanics 554 (2006) 299–322.
[2] H.E. Huppert, A.W. Woods, Gravity-driven flows in porous layers, Journal of Fluid Mechanics 292 (1995) 55–69.
[3] S. Lyle, H.E. Huppert, M. Hallworth, M. Bickle, A. Chadwick, Axisymmetric gravity currents in a porous medium, Journal of Fluid Mechanics 543 (2005) 293–302.
[4] D. Vella, H.E. Huppert, Gravity currents in a porous medium at an inclined plane, Journal of Fluid Mechanics 555 (2006) 353–362.
[5] M. Golding, H.E. Huppert, The effect of confining impermeable boundaries on gravity currents in a porous medium, Journal of Fluid Mechanics 649 (2010) 1–17.
[6] D. Pritchard, A.W. Woods, A.J. Hogg, On the slow draining of a gravity current moving through a layered permeable medium, Journal of Fluid Mechanics 444 (2001) 23–47.
[7] J.A. Neufeld, D. Vella, H.E. Huppert, The effect of a fissure on storage in a porous medium, Journal of Fluid Mechanics 639 (2009) 239–259.
[8] S.E. Gasda, H.M. Nilsen, H.K. Dahle, W.G. Gray, Effective models for CO_2 migration in geological systems with varying topography, Water Resources Research 48 (2012) W10546.
[9] J.P. Pascal, H. Pascal, Similarity solutions to gravity flows of non-Newtonian fluids through porous media, International Journal of Non-Linear Mechanics 28 (2) (1993) 157–167.
[10] V. Di Federico, R. Archetti, S. Longo, Similarity solutions for spreading of a two-dimensional non-Newtonian gravity current in a porous layer, Journal of Non-Newtonian Fluid Mechanics 177–178 (2012) 46–53.
[11] S.C.M. Krevor, R. Pini, B. Li, S.M. Benson, Capillary heterogeneity trapping of CO_2 in a sandstone rock at reservoir conditions, Geophysical Research Letters 38 (2011) L15401, http://dx.doi.org/10.1029/2011GL048239.
[12] S.E. King, A.W. Woods, Dipole solutions for viscous gravity currents: theory and experiments, Journal of Fluid Mechanics 483 (2003) 91–109.
[13] D. Zheng, B. Soh, H.E. Huppert, H.A. Stone, Fluid drainage from the edge of a porous reservoir, Journal of Fluid Mechanics 718 (2013) 558–568.
[14] X.-W. Jiang, L. Wan, X.-S. Wang, S. Ge, J. Liu, Effect of exponential decay in hydraulic conductivity with depth on regional groundwater flow, Geophysical Research Letters 36 (2009) L24402, http://dx.doi.org/10.1029/2009GL041251.
[15] G. De Marsily, Quantitative Hydrogeology, Academic Press, Dordrecht, 1986.
[16] A. Altunkaynak, Steady-state groundwater flow model with variable hydraulic conductivity, Hydrological Sciences Journal 52 (1) (2007) 221–229.
[17] A. Altunkaynak, Z. Sen, Steady state flow with hydraulic conductivity change around large diameter wells, Hydrological Processes 25 (2011) 1778–1783.
[18] H.-D. Yeh, C.-C. Kuo, An analytical solution for heterogeneous and anisotropic anticline reservoirs under well injection, Advances in Water Resources 33 (2010) 419–429.
[19] J.S. Mathunjwa, A.J. Hogg, Freely draining gravity currents in porous media: dipole self-similar solutions with and without capillary retention, European Journal of Applied Mathematics 18 (2007) 337–362.
[20] R.E. Pattle, Diffusion from an instantaneous point source with a concentration dependent coefficient, Quarterly Journal of Mechanics and Applied Mathematics 12 (4) (1959) 407–409.
[21] D. Takagi, H.E. Huppert, Viscous gravity currents inside confining channels and fractures, Physics of Fluids 20 (2008) 023104.
[22] C.W. Fetter, Contaminant Hydrogeology, 2nd ed., Prentice Hall, New York, 1999.
[23] D. Silin, T.W. Patzek, S.M. Benson, A one-dimensional model of vertical gas plume migration through a heterogeneous porous medium, International Journal of Greenhouse Gas Control 3 (2009) 300–310.